

# Inverse Seesaw Mechanism and Axion Portal Fermionic Dark Matter

---

Nakorn Thongyoi,<sup>a</sup> Patipan Uttayarat,<sup>b</sup> and Chakrit Pongkitivanichkul<sup>a</sup>

<sup>a</sup>*Khon Kaen Particle Physics and Cosmology Theory Group (KKPaCT),  
Department of Physics, Faculty of Science, Khon Kaen University,  
123 Mitraphap Rd, Khon Kaen 40002, Thailand*

<sup>b</sup>*Theoretical High-Energy Physics and Astrophysics Research Unit (ThEPA), Department of Physics,  
Srinakharinwirot University, 114 Sukhumvit 23 Rd.,  
Wattana, Bangkok 10110, Thailand*

*E-mail:* [nakorn.thongyoi@gmail.com](mailto:nakorn.thongyoi@gmail.com), [patipan@g.swu.ac.th](mailto:patipan@g.swu.ac.th),  
[chakpo@kku.ac.th](mailto:chakpo@kku.ac.th)

**ABSTRACT:** We propose a minimal extension of the Standard Model (SM) that addresses both the smallness of neutrino masses and the dark matter (DM) puzzle via the inverse seesaw mechanism and an axion portal fermionic DM. This model generates light neutrino masses without requiring high energy scales, enhancing its testability in future collider experiments. An axion-like particle (ALP) connects the SM and DM sectors, yielding a distinct phenomenology. Our analysis shows that the model is consistent with constraints from neutrino oscillations and DM relic density as well as satisfying the current measurement on muon  $g - 2$ . This work offers a unified framework to address neutrino masses and DM, with implications for particle physics and cosmology.

---

# Contents

<b>1</b>	<b>Introduction</b>	<b>1</b>
<b>2</b>	<b>The model</b>	<b>2</b>
2.1	The scalar sector . . . . .	3
2.2	The neutrino sector . . . . .	4
2.3	Dark matter sector . . . . .	6
2.4	The axion interactions . . . . .	6
<b>3</b>	<b>Phenomenology</b>	<b>6</b>
3.1	Neutrino masses and mixing . . . . .	7
3.2	Dark matter phenomenology . . . . .	9
3.3	The measurement of muon magnetic moment . . . . .	9
<b>4</b>	<b>Numerical results</b>	<b>11</b>
<b>5</b>	<b>Conclusion and discussion</b>	<b>14</b>

---

## 1 Introduction

The Standard Model (SM) has been a cornerstone in understanding elementary particles and their interactions. Despite its successes, certain phenomena remain unexplained, notably the non-zero masses of neutrinos and the existence of dark matter (DM). The SM’s failure to accommodate these observations has driven significant efforts to extend it, leading to a range of proposed mechanisms and models.

One of the most profound issues with the SM is its prediction of massless neutrinos. However, experimental evidence from Super-Kamiokande [1], SNO [2], KamLAND [3], Daya Bay [4], RENO[5], CHOOZ [6], K2K [7], T2K[8], and LSND [9] confirms that neutrinos undergo flavor oscillations, and hence are massive. Traditional seesaw mechanisms have been proposed to explain the smallness of neutrino masses by introducing heavy right-handed Majorana neutrinos, which generate light neutrino masses suppressed by the heavy Majorana scale [10–15], commonly referred to as the seesaw scale. However, the traditional seesaw mechanism usually requires a seesaw scale around  $M \sim 10^{12}$  GeV, which greatly reduces the possibility to probe the model experimentally. On the other hand, the inverse seesaw model [16–24] offers a more testable neutrino mass generation mechanism. In this scenario, sterile neutrinos with small, yet technically natural, lepton number-violation (LNV) couplings are introduced. These small LNV couplings help to lower the seesaw scale down to within reach of colliders. This approach has gained traction as a realistic and testable framework, with studies exploring its implications on lepton flavor violation (LFV) and collider phenomenology [17, 25–32].

On the other hand, the existence of DM has been firmly established through astrophysical observations, such as galaxy rotation curves [33, 34] and cosmic microwave background measurements [35–37]. Various extensions of the SM have been proposed to accommodate DM, see Ref. [38–43] for recent reviews. One of the most studied scenario is the Higgs portal DM [44], thanks to its simplicity and predictive nature. In this framework, the Higgs boson serves as a mediator between the DM and the SM sector. Phenomenology of the Higgs portal DM has been studied in Ref. [45–47]. Due to its minimal structure, the Higgs portal model cannot accommodate neutrino masses without a further extension.

An alternative and compelling approach is the axion portal model, which introduces an axion or axion-like particle (ALP) as a mediator between the DM and the SM sectors. Initially proposed to address the strong CP problem in quantum chromodynamics, axion has gained interest in DM studies due to their weak interactions and stability [48–50]. ALP portal models offers unique signatures in indirect detection experiment, cosmic microwave background distortions, and low energy precision measurements, which can differentiate them from Higgs portal models [51–54]. It is also interesting to note that ALP can be connected to neutrino mass generation models as well [55].

Another historically interesting observable is the muon anomalous magnetic moment,  $g - 2$ , whose precise measurements at Fermilab [56, 57] and previously at Brookhaven [58] have long appeared to deviate from earlier SM predictions [59]. This tension, which once stood at nearly  $5\sigma$ , motivated significant theoretical and experimental efforts. However, a recent comprehensive update by the Muon  $g - 2$  Theory Initiative [60], incorporating improved lattice QCD evaluations and addressing tensions in  $e^+e^-$  data, has led to a revised SM prediction that is in agreement with the experimental average within uncertainties [61]. While the anomaly is no longer statistically significant, the muon magnetic moment remains a sensitive probe for new physics.

In this work, we build upon these developments by proposing a minimal SM extension that combines the inverse seesaw mechanism for neutrino mass generation and the ALP portal DM. Our model draws from the previous study that explored Higgs portals in the DM-neutrino mass model [62], aiming instead to utilize the ALP portal [63–73], which offers new dynamics and observables. In this work, we also apply the recent constraint [60] on muon  $g - 2$  to the ALP portal model, which place a non-trivial constraint on the model parameter space. This approach not only addresses the neutrino mass and DM issues within a unified framework but also proposes testable signatures that could guide future experimental searches.

The paper is organised as follows. The model and particle contents are discussed in detail in section 2. In section 3, we discuss the model phenomenology and relevant constraints. Numerical results are presented in section 4. Finally, we summarise our findings and express an outlook in section 5.

## 2 The model

In this work, we propose an extension to the SM with an electroweak (EW) singlet complex scalar ( $\Phi$ ), two EW singlet right-handed heavy neutrinos ( $N_R^i$ ), two EW singlet left-handed

heavy neutrinos ( $S_L^I$ ), a pair of fermionic dark matter ( $\chi_L$  and  $\chi_R$ ).<sup>1</sup> In addition, the chiral  $U(1)_{PQ}$  global symmetry is imposed to stabilise the DM sector, and is assumed to be broken at a scale higher than the EW symmetry breaking scale. The relevant particle contents and their charge assignment under  $SU(2)_L \times U(1)_Y \times U(1)_{PQ}$  is summarised in Tab. 1. With this charge assignment, the model does not generate the axion coupling to any SM gauge boson through the triangle diagram of fermions. There is only axion-fermion coupling which is naturally generated by the PQ transformation on the kinetic term of fermions.

	$SU(2)_L$	$U(1)_Y$	$U(1)_{PQ}$
$L_L$	<b>2</b>	$-1/2$	0
$e_R$	1	$-1$	$-X_H$
$Q_L$	<b>2</b>	$1/6$	0
$u_R$	1	$2/3$	$X_H$
$d_R$	1	$-1/3$	$-X_H$
$H$	<b>2</b>	$+1/2$	$X_H$
$N_R$	1	0	$X_H$
$S_L$	1	0	$X_\Phi + X_H$
$\chi_{L,R}$	1	0	$0, -X_\Phi$
$\Phi$	1	0	$X_\Phi$

**Table 1:** The charge assignment under the electroweak and  $U(1)_{PQ}$  groups.

## 2.1 The scalar sector

The scalar potential consistent with  $U(1)_{PQ}$  is given by

$$V(H, \Phi) = -\mu_H^2 H^\dagger H + \lambda_H (H^\dagger H)^2 - \mu_\Phi^2 \Phi^\dagger \Phi + \lambda_\Phi (\Phi^\dagger \Phi)^2 + \lambda_{H\Phi} (H^\dagger H) (\Phi^\dagger \Phi). \quad (2.1)$$

The field  $H$  and  $\Phi$  can be expanded as

$$H = \frac{1}{\sqrt{2}} \begin{pmatrix} \sqrt{2}G^+ \\ v_h + h' + iG^0 \end{pmatrix}, \quad \Phi = \frac{1}{\sqrt{2}} (v_\phi + \phi') e^{ia/v_\phi}, \quad (2.2)$$

where  $G^+$  and  $G^0$  are the would-be Goldstone bosons.  $v_h$  and  $v_\phi$  are the vacuum expectation values (vev) of  $H$  and  $\Phi$  respectively and  $f_a$  is the ALP decay constant. Since  $U(1)_{PQ}$  is assumed to be broken at scale higher than the EW scale, we have  $v_\phi, f_a > v_h$ . Note that we employ the non-linear parametrization for  $\Phi$  which makes the ALP,  $a$ , appears explicitly as the phase. The fields  $h'$  and  $\phi'$  mix to form the mass eigenstates

$$\begin{pmatrix} h \\ \phi \end{pmatrix} = \begin{pmatrix} \cos \theta & \sin \theta \\ -\sin \theta & \cos \theta \end{pmatrix} \begin{pmatrix} h' \\ \phi' \end{pmatrix}, \quad (2.3)$$

<sup>1</sup>Scenarios with one  $N_R$  and one  $S_L$ , or one  $N_R$  and two  $S_L$  lead to two vanishing light neutrino masses. Scenario with two  $N_R$  and one  $S_L$  is compatible with neutrino oscillation data. However, it would require more free parameters than the scenario presented in this work.

where

$$\tan(2\theta) = \frac{\lambda_{H\Phi} v_h v_\phi}{\lambda_\Phi v_\phi^2 - \lambda_H v_h^2}. \quad (2.4)$$

Here we identify the field  $h$  with the 125 GeV Higgs boson. The masses of  $h$  and  $\phi$  are given by

$$m_{h,\phi}^2 = \lambda_H v_h^2 + \lambda_\Phi v_\phi^2 \mp \sqrt{(\lambda_\Phi v_\phi^2 - \lambda_H v_h^2)^2 + \lambda_{H\Phi}^2 v_h^2 v_\phi^2}. \quad (2.5)$$

It is more convenient to express the quartic couplings  $\lambda_H$ ,  $\lambda_\Phi$ , and  $\lambda_{H\Phi}$  in terms of the vevs, the masses and the mixing angle. They are given by

$$\begin{aligned} \lambda_H &= \frac{m_h^2 \cos^2 \theta + m_\phi^2 \sin^2 \theta}{v_h^2}, \\ \lambda_\Phi &= \frac{m_h^2 \sin^2 \theta + m_\phi^2 \cos^2 \theta}{v_\phi^2}, \\ \lambda_{H\Phi} &= \frac{(m_\phi^2 - m_h^2) \sin \theta \cos \theta}{v_h v_\phi}. \end{aligned} \quad (2.6)$$

Thus, the scalar potential can be described by three free parameters:  $v_\phi$ ,  $m_\phi$  and  $\sin \theta$ . We note that  $\sin \theta$  is constrained by the 125 GeV Higgs boson measurement. The latest results from the ATLAS and CMS collaborations place an upper bound on  $\sin \theta \leq 0.15$  [74, 75].

The ALP potential, on the other hand, is generated from the non-perturbative effect, which breaks  $U(1)_{PQ}$  into a shift symmetry,  $a \rightarrow a + f_a$ . This shift symmetry dictates that the ALP potential takes the form of the instanton cosine potential [76]

$$V(a) = \tilde{\Lambda}_a^4 \left[ 1 - \cos \left( \frac{2\pi a}{f_a} \right) \right], \quad (2.7)$$

where  $\tilde{\Lambda}_a^4$  is the maximum value of the potential. By identifying this shift under  $U(1)_{PQ}$  transformation with the period of the ALP potential, one obtains a relation

$$f_a = X_\Phi v_\phi. \quad (2.8)$$

The ALP potential also generates the ALP mass

$$m_a^2 = \frac{\Lambda_a^4}{f_a}, \quad (2.9)$$

where  $\Lambda_a^2 \equiv 2\pi \tilde{\Lambda}_a^2$ .

## 2.2 The neutrino sector

In this section, we derive the light neutrino mass matrix in the inverse seesaw scenario. The Yukawa interactions consistent with the global  $U(1)_{PQ}$  are given by

$$\mathcal{L}_{Yuk} \supset -Y^{\alpha i} \bar{L}_L^\alpha \tilde{H} N_R^i - Y'^{Ii} \Phi \bar{S}_L^I N_R^i + \text{h.c.}, \quad (2.10)$$

where  $\alpha, i$ , and  $I$  are generation indices, and  $\tilde{H} = i\sigma_2 H^*$ . These interactions by themselves do not violate lepton number, and hence cannot generate neutrino mass. Thus, we also introduce the LNV Majorana mass terms

$$\mathcal{L}_{Maj.} = -\frac{\mu_R^{ij}}{2} \overline{N_R^c}^i N_R^j - \frac{\mu_S^{IJ}}{2} \overline{S_L^c}^I S_L^J + \text{h.c.}, \quad (2.11)$$

where  $\psi^c = C\overline{\psi}^T$  is the charge conjugated field. The  $\mu_R$  and  $\mu_S$  terms also break  $U(1)_{PQ}$  softly. However, they are expected to be small thanks to 't Hooft technical naturalness argument. After  $U(1)_{PQ}$  and EW symmetry breaking, Eq. (2.10) and (2.11) lead to the neutrino mass terms

$$\begin{aligned} -\mathcal{L}_{\text{mass}}^\nu &= m_D^{\alpha i} \overline{\nu_L^\alpha} N_R^i + M_N^{Ij} \overline{S_L^I} N_R^j \\ &+ \frac{\mu_R^{ij}}{2} \overline{N_R^c}^i N_R^j + \frac{\mu_S^{IJ}}{2} \overline{S_L^c}^I S_L^J + \text{h.c.}, \end{aligned} \quad (2.12)$$

where we define  $m_D^{\alpha i} = Y^{\alpha i} v_h / \sqrt{2}$  and  $M_N^{Ij} = Y^{Ij} v_\phi / \sqrt{2}$ . The neutrino mass terms can be written in a compact form

$$-\mathcal{L}_{\text{mass}}^\nu = \frac{1}{2} \overline{\mathcal{N}_R^c} \mathcal{M}_\nu \mathcal{N}_R + \text{h.c.}, \quad (2.13)$$

where

$$\mathcal{N}_R = \begin{pmatrix} \nu_L^c \\ N_R \\ S_L^c \end{pmatrix}, \quad \mathcal{M}_\nu = \begin{pmatrix} \mathbf{0} & m_D & \mathbf{0} \\ m_D^T & \mu_R & M_N^T \\ \mathbf{0} & M_N & \mu_S \end{pmatrix}. \quad (2.14)$$

The neutrino mass matrix  $\mathcal{M}_\nu$  can be brought to a block diagonal form by [15]

$$V^T \mathcal{M}_\nu V = \begin{pmatrix} (M_{\text{light}})_{3 \times 3} & \mathbf{0} \\ \mathbf{0} & (M_{\text{heavy}})_{4 \times 4} \end{pmatrix}, \quad (2.15)$$

where  $V$  is a unitary matrix,  $M_{\text{light}}$  and  $M_{\text{heavy}}$  are the light neutrino and heavy neutrino mass matrices respectively. In the limit where  $\|\mu_R\|, \|\mu_S\| \ll \|m_D\| \ll \|M_N\|$ <sup>2</sup>,  $M_{\text{light}}$  can be approximated by

$$M_{\text{light}} \simeq -m_D M_N^{-1} \mu_S (M_N^T)^{-1} m_D^T. \quad (2.16)$$

Note that, to lowest order, the Majorana mass term  $\mu_R$  does not contribute to  $M_{\text{light}}$ . Notice also that in this case,  $M_{\text{light}}$  receives an extra suppression of order  $\|\mu_S\|/\|M_N\|$  compared to the usual seesaw scenario. This makes it possible to place a seesaw scale within reach of collider experiment.

---

<sup>2</sup>Here we define  $\|M\| \equiv \sqrt{\text{Tr}(M^\dagger M)}$ .

### 2.3 Dark matter sector

The dynamics of the DM sector is governed by the Yukawa interaction

$$\mathcal{L}_{DM} = -g_\chi \Phi \overline{\chi} L \chi_R + \text{h.c.} \quad (2.17)$$

The  $U(1)_{PQ}$  symmetry breaking generates a DM mass,  $m_\chi = g_\chi v_\phi / \sqrt{2}$ . Below the  $U(1)_{PQ}$  breaking scale, DM interactions are given by

$$\begin{aligned} \mathcal{L}_{DM} \supset & -\frac{m_\chi}{v_\phi} \sin \theta h \overline{\chi} \chi - \frac{m_\chi}{v_\phi} \cos \theta \phi \overline{\chi} \chi - i \frac{m_\chi}{v_\phi} a \overline{\chi} \gamma_5 \chi \\ & - i \frac{g_\chi \cos \theta}{\sqrt{2} v_\phi} a \phi \overline{\chi} \chi - i \frac{g_\chi \sin \theta}{\sqrt{2} v_\phi} a h \overline{\chi} \chi, \end{aligned} \quad (2.18)$$

where  $\theta$  is the neutral scalars mixing angle defined in Eq. (2.4).

From the above interaction, one see that the  $h$ ,  $\phi$  and  $a$  can serve as a portal between the DM sector and the SM sector. However, the  $h$  and  $\phi$  portal to SM fermions and gauge bosons are suppressed by  $\sin^2 2\theta \lesssim 0.08$  due to the mixing in the neutral scalar sector. The ALP portal, on the other hand, does not suffer from this suppression. For simplicity, we will assume  $\theta = 0$  in this work. Thus, DM phenomenology is mediated by the ALP portal.

### 2.4 The axion interactions

The interaction term of axion-fermion and axion-photon can be derived by demanding that the Lagrangian of the model is invariant under the following PQ transformation

$$f_R \mapsto e^{-iX_f a/f_a} f_R, \quad \psi_R \mapsto e^{-iX_\psi a/f_a} \psi_R, \quad \varphi \mapsto e^{-iX_\varphi a/f_a} \varphi, \quad (2.19)$$

where  $f$  is the SM fermion,  $\psi = \{\chi, N\}$  and  $\varphi = \{H, \Phi\}$ . The  $X_f$  and  $X_\varphi$  are PQ-charges of fermions and scalars respectively. According to table 1, the PQ transformation (2.19) on the kinetic term of SM fermions leads to axion-SM fermion derivative interactions in the form of

$$\mathcal{L}_{\text{kin}} \supset \bar{f} i \gamma^\mu \partial_\mu f \rightarrow \bar{f} i \gamma^\mu \partial_\mu f + C_{ff} \frac{\partial_\mu a}{f_a} \bar{f} \gamma^\mu \gamma_5 f, \quad (2.20)$$

where  $C_{ff} = X_f = \pm X_\varphi$  where  $+$  is for up-type quarks and  $-$  is for charged lepton and down-type quarks.

## 3 Phenomenology

In this section, we study the phenomenology of our model. We are interested in the minimal scenario, in the sense of the least number of free parameters, which could explain 1) neutrino masses and mixing, 2) dark matter relic density, and 3) the muon  $g - 2$  measurement consistently.

### 3.1 Neutrino masses and mixing

In our scenario  $m_D$  is a complex  $3 \times 2$  matrix,  $M_N$  is a complex  $2 \times 2$  matrix and  $\mu_S$  is a symmetric complex  $2 \times 2$  matrix. However, not all components of these matrices are physical. One can perform unitary field redefinitions on  $N_R^i$  and  $S_L^I$  to put  $M_N$  and  $\mu_S$  in the form

$$m_N \sim \text{diag.}(1, \gamma), \quad (3.1)$$

$$\mu_S \sim \begin{pmatrix} 1 & \alpha\gamma \\ \alpha\gamma\beta\gamma^2 & e^{i\phi} \end{pmatrix}, \quad (3.2)$$

where  $\gamma$ ,  $\alpha$ ,  $\beta$  and  $\phi$  are real and positive. Note that our parametrization of  $m_N$  and  $\mu_S$  makes explicit that  $\gamma$  drops out from the light neutrino mass matrix. In the above equations, we have also factored out the 1-1 components from both  $m_N$  and  $\mu_S$ . Moreover, by redefining the phases of  $L^\alpha$  and  $N^i$ , one can rotate away 4 phases in  $m_D$ . From our analysis, we find two minimal textures of  $m_D$ , which lead to viable neutrino masses and mixing. They are

$$m_D^{(A)} \sim \begin{pmatrix} 1 & 0 \\ y_1 y_2 & \\ 0 & y_3 \end{pmatrix}, \quad (3.3)$$

$$m_D^{(B)} \sim \begin{pmatrix} 1 & 0 \\ 0 & y_1 \\ y_2 y_3 & \end{pmatrix}, \quad (3.4)$$

where  $y_i > 0$ . Again, we have factored out the 1-1 component of  $m_D$ .

Finally, the light neutrino mass matrix are given by

$$M_{\text{light}}^{(A)} = \kappa \begin{pmatrix} 1 & y_1 + \alpha y_2 & \alpha y_3 \\ y_1 + \alpha y_2 y_1^2 + 2\alpha y_1 y_2 + \beta e^{i\phi} y_2^2 \alpha y_1 y_3 + \beta e^{i\phi} y_2 y_3 & & \\ \alpha y_3 & \alpha y_1 y_3 + \beta e^{i\phi} y_2 y_3 & \beta e^{i\phi} y_3^2 \end{pmatrix}, \quad (3.5)$$

$$M_{\text{light}}^{(B)} = \kappa \begin{pmatrix} 1 & \alpha y_1 & y_2 + \alpha y_3 \\ \alpha y_1 & \beta e^{i\phi} y_1^2 & \alpha y_1 y_2 + \beta e^{i\phi} y_1 y_3 \\ y_2 + \alpha y_3 \alpha y_1 y_2 + \beta e^{i\phi} y_1 y_3 y_2^2 + 2\alpha y_2 y_3 + \beta e^{i\phi} y_3^2 & & \end{pmatrix}, \quad (3.6)$$

where  $\kappa \sim v^2 \|\mu_S\| / f_a^2$  is the overall scale of neutrino masses. Thus, in our scenario,  $M_{\text{light}}$  depends on 7 real parameters:  $\kappa$ ,  $y_{1,2,3}$ ,  $\alpha$ ,  $\beta$ , and  $\phi$ .

The light neutrino mass matrix can be diagonalized by a unitary matrix  $U$ ,

$$U^T M_{\text{light}} U = \text{diag.}(m_1, m_2, m_3), \quad (3.7)$$

where  $m_i > 0$  are the mass eigenvalues. The above equation defines the Pontecorvo–Maki–Nakagawa–Sakata (PMNS) matrix. In general, the PMNS matrix contains three mixing angles, one Dirac phase, and two Majorana phases.

Parameters	Normal Ordering	Inverted Ordering
$\sin^2 \theta_{12}$	$0.308^{+0.037}_{-0.033}$	$0.308^{+0.037}_{-0.033}$
$\sin^2 \theta_{13}$	$0.02215^{+0.00173}_{-0.00185}$	$0.02231^{+0.00178}_{-0.00171}$
$\sin^2 \theta_{23}$	$0.470^{+0.115}_{-0.035}$	$0.550^{+0.034}_{-0.110}$
$m_{\text{solar}}^2/10^{-5} \text{ eV}^{-2}$	$7.49^{+0.56}_{-0.57}$	$7.49^{+0.56}_{-0.57}$
$m_{\text{atm}}^2/10^{-3} \text{ eV}^{-2}$	$2.513^{+0.065}_{-0.062}$	$2.484^{+0.063}_{-0.063}$
$\delta_{\text{CP}}/^\circ$	$212^{+152}_{-88}$	$274^{+61}_{-73}$

**Table 2:** The best fit values of neutrino oscillation parameters and their  $3\sigma$  ranges as determined from the global neutrino data [77]. Here  $m_{\text{solar}}^2 = m_2^2 - m_1^2$  and  $m_{\text{atm}}^2 = m_3^2 - m_1^2$  ( $m_2^2 - m_3^2$ ) for normal ordering (inverted ordering).

Once the neutrino mass matrix  $M_{\text{light}}$  has been diagonalized, the three mixing angles can be determined by

$$s_{13}^2 = |U_{e3}|^2, \quad s_{12}^2 = \frac{|U_{e2}|^2}{1 - |U_{e3}|^2}, \quad s_{23}^2 = \frac{|U_{\mu 3}|^2}{1 - |U_{e3}|^2}, \quad (3.8)$$

where  $s_{ij} = \sin \theta_{ij}$  is the sine of the mixing angles. The Dirac phase,  $\delta_{\text{CP}}$ , is encoded in the Jarlskog invariant

$$J = \text{Im} (U_{\mu 3} U_{e3}^* U_{e2} U_{\mu 2}^*) = c_{12} s_{12} c_{23} s_{23} c_{13}^2 s_{13} \sin \delta_{\text{CP}}. \quad (3.9)$$

The remaining two Majorana phases, in principle, can be deduced from the invariants  $\text{Im}[(U_{e2} U_{e1}^*)^2]$  and  $\text{Im}[(U_{e3} U_{e1}^*)^2]$  [78]. However, both Majorana phases have never been determined experimentally. The values of neutrino masses, mixing angles, and the Dirac phase, as determined from the global analysis of neutrino data, are collected in Tab. 2.

An interesting feature of our set up is that the light neutrino mass matrix is rank 2. As a result, the lightest neutrino mass is vanishing. Hence, the other two non vanishing neutrino masses depend only on  $\Delta m_{\text{sol}}^2$  and  $\Delta m_{\text{atm}}^2$ . In particular, the sum of neutrino masses is given by  $\sum_i m_i = \sqrt{\Delta m_{\text{sol}}^2} + \sqrt{\Delta m_{\text{atm}}^2}$  and  $\sqrt{\Delta m_{\text{atm}}^2 - \Delta m_{\text{sol}}^2} + \sqrt{\Delta m_{\text{atm}}^2}$  for the NO and IO scenarios respectively. The sum of neutrino masses is constrained by cosmological measurement. Combining the Planck 2018 cosmic microwave background data and the baryonic acoustic oscillation measurement result in an upper bound  $\sum_i m_i \leq 130 \text{ meV}$  at 95% confidence level (CL) [35]. In addition to the neutrino masses sum, there are two effective masses relevant for laboratory based neutrino experiments. First, the effective mass  $m_{\nu_e}^{\text{eff}} = \sqrt{\sum_i |U_{ei}|^2 m_i^2}$  determines the endpoint of beta decay spectrum. The latest measurement published by KATRIN has put an upper bound of  $m_{\nu_e}^{\text{eff}} \leq 450 \text{ meV}$  at 90% CL [79]. Second the rate for neutrinoless double beta ( $0\nu\beta\beta$ ) decay depends on the effective mass  $m_{ee} = |\sum_i U_{ei}^2 m_i|$ . The strongest upper bound on  $m_{ee}$  is provided by the KamLAND-Zen experiment with  $m_{ee} \leq 36 - 156 \text{ meV}$  at 90% CL [80].

### 3.2 Dark matter phenomenology

In addition to generating neutrino masses, our model also provides a DM candidate which is assumed to be a fermion,  $\chi$ . In the absence of the neutral scalar mixing,  $\theta$ , DM interaction with the SM sector is mediated by the ALP, see Eq. (2.18) and (2.20). Moreover, this model gives additional contribution apart from the SM one which needs to be constrained by the muon  $g - 2$  measurement, see Sec. 3.3. As a result, assuming  $\phi$  and  $a$  are heavier than  $\chi$ , there are nine DM annihilation channels: one of the nine annihilation processes  $\chi\bar{\chi} \rightarrow f\bar{f}$ . Therefore, the total annihilation cross section reads

$$\langle\sigma v_{\text{rel}}\rangle = \sum_f \langle\sigma_{f\bar{f}} v_{\text{rel}}\rangle \quad (3.10)$$

where

$$\langle\sigma_{f\bar{f}} v_{\text{rel}}\rangle \simeq \frac{8}{\pi} \frac{C_{ff}^2 X_\Phi^4 m_f^2 m_\chi^4}{(m_a^2 - 4m_\chi^2)^2 f_a^4} \sqrt{1 - \frac{m_f^2}{m_\chi^2}}. \quad (3.11)$$

Here  $m_f$  and  $m_a$  are the SM fermion and axion masses, respectively. The  $C_{ff}$  is the axion-SM fermion coupling and  $X_\Phi$  is the  $f_a/v_\Phi$  ratio.

The energy density of DM is precisely measured by the Planck satellite [35] to be

$$\Omega_{\text{DM}}^{\text{Planck}} h^2 = 0.12 \pm 0.0012. \quad (3.12)$$

Assuming DM is present in the thermal bath of the early Universe, its present energy density is related to its annihilation cross section. The value of DM energy density can be determined by solving Boltzman equation numerically. However, here we will adopt a simple freeze out approximation, which yields the thermal relic cross section  $\langle\sigma v_{\text{rel}}\rangle = 2.6 \times 10^{-26} \text{ cm}^3/\text{s}$ . In our numerical analysis, we take  $\pm 0.4 \times 10^{-26} \text{ cm}^3/\text{s}$  as the nominal error associate with the approximation. The thermal relic cross section, in turns, constrains the possible range of the ALP couplings  $C_{ff}$ .

### 3.3 The measurement of muon magnetic moment

The recent report on the measurement of muon magnetic moment [60, 61] has been confirmed that the measured value agrees with the SM prediction

$$\Delta a_\mu \equiv a_\mu^{\text{EXP}} - a_\mu^{\text{SM}} = (39 \pm 64) \times 10^{-11}, \quad (3.13)$$

where  $a_\mu = (g - 2)/2$ . There is no tension between measurement and the SM prediction now. We can use this constraint to find the allowed parameter space on  $C_{ff}/f_a$ .

In this model, the additional contributions to  $a_\mu$  can be induced by ALP-SM fermion couplings

$$\mathcal{L} \supset \frac{C_{ff}}{f_a} (\partial_\mu a) \bar{f} \gamma^\mu \gamma_5 f,$$

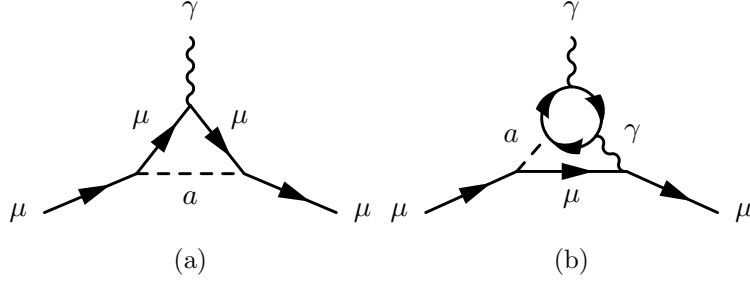


**Figure 1:** The representative diagrams for axion contribution to muon  $g - 2$ . The left and middle panels are one-loop contribution while the right is the two-loop one.

through the Feynman diagrams shown in Fig. 1. The analytical result for each diagram is given by [81, 82]

$$\begin{aligned}\Delta a_\mu^{(a)} &= -\frac{1}{8\pi^2} \left( \frac{C_{ff}}{f_a} \right)^2 m_\mu^2 \int_0^1 dx \frac{m_\mu^2 x^3}{m_a^2(1-x) + m_\mu^2 x^2}, \\ \Delta a_\mu^{(b)} &= \frac{\alpha}{8\pi^3} \left( \frac{C_{ff}}{f_a} \right)^2 m_\mu^2 \left( (I_e + I_\mu + I_\tau + 3I_d + 3I_s + 3I_b) \right. \\ &\quad \left. - (3I_u + 3I_c + 3I_t) \right),\end{aligned}\tag{3.14}$$

where

$$I_f(m_a, m_f) = \int_0^1 dx \frac{m_f^2}{m_f^2 + m_a^2 x(1-x)} \log \left[ \frac{m_f^2}{m_a^2 x(1-x)} \right].\tag{3.15}$$

The total anomalous magnetic moment of the muon is then given by

$$\Delta a_\mu = \Delta a_\mu^a + \Delta a_\mu^b\tag{3.16}$$

It should be noted that diagrams 1 (a) generate a negative contribution while diagrams 1 (b) can give either negative or positive ones depending on the axion mass and  $C_{ff}$ . However, the total muon  $a_\mu$  changes the sign at the axion mass around 500-600 GeV as shown in Fig.2. In that figure, we made a plot of  $\Delta a_\mu$  as a function of axion mass for various values of  $C_{ff} = \{100, 500, 1000, 5000, 10000\}$  to compare the effect of  $C_{ff}/f_a$  on  $\Delta a_\mu$ . Two horizontal lines correspond to the upper and lower limits recently reported by [60, 61]. For  $C_{ff} = 100$  or  $C_{ff}/f_a = 10^{-2}$ , we find that the contribution from new diagram has only a mild effect so that the  $\Delta a_\mu$  is within the range of measurement within  $\pm\sigma$  for a range of mass from  $\{1, 10^4\}$  GeV. For the larger  $C_{ff}/f_a$ , the smaller allowed range of mass. In addition, the additional  $\Delta a_\mu$  changes a sign at around 600 GeV.

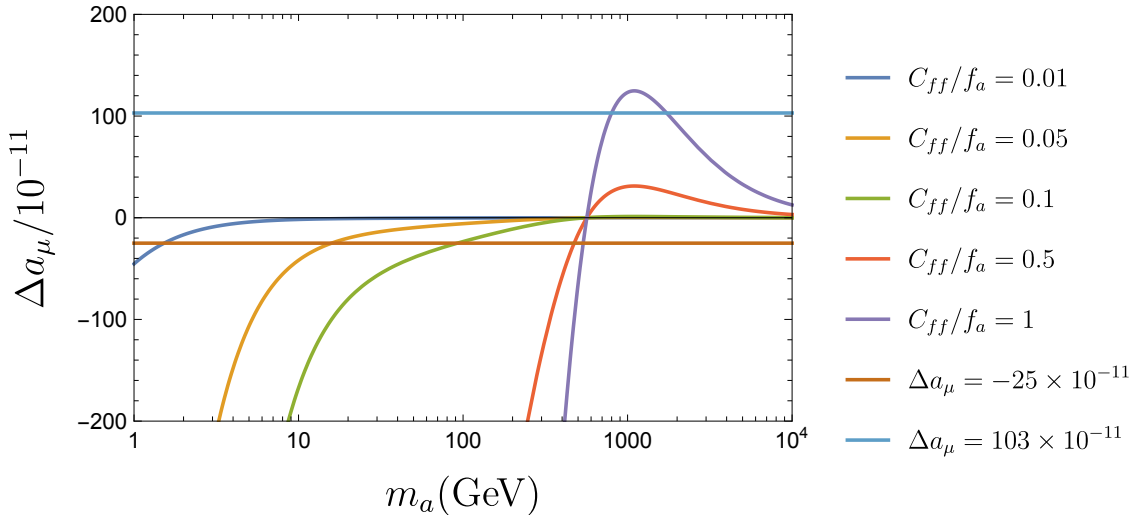


**Figure 2:** The  $a_\mu$  plot as a function of  $m_a$  for various values of  $C_{ff}$  (see legends). Two horizontal lines correspond to upper and lower limits for recent measurement.

#### 4 Numerical results

In this section, we perform the numerical scan on the model parameter space. In our setup, the free parameters can be divided into two groups— neutrino, and DM and muon  $g-2$ . We first analyze the neutrino sector which depend on 7 free parameters. The free parameters are varied within the following ranges:

$$1 \text{ meV} \leq \kappa \leq 1 \text{ eV}, \quad 10^{-3} \leq y_i, a, b \leq 10^3, \quad 0 \leq \phi \leq 2\pi. \quad (4.1)$$

We search for the region of parameter space which is consistent with the neutrino oscillation data at the  $3\sigma$  level. We then deduce the corresponding values for  $\sum_i m_i$ ,  $m_{\nu_e}^{\text{eff}}$ , and  $m_{ee}$ .

Texture	$\delta_{\text{CP}} [^\circ]$	$\sum_i m_i$ [meV]	$m_{\nu_e}^{\text{eff}}$ [meV]	$m_{ee}$ [meV]
A	124.16–289.95	58.09–59.21	8.64–9.00	1.16–3.04
B	124.18–289.93	58.25–59.20	8.69–9.14	1.85–4.01

**Table 3:** The range of  $\delta_{\text{CP}}$ ,  $\sum m_i$ ,  $m_{\nu_e}^{\text{eff}}$  and  $m_{ee}$  in each scenario.

We find both  $m_D^{(A)}$  and  $m_D^{(B)}$  can only accommodate NO neutrino masses. As a result, we have  $\sum_i m_i = \sqrt{\Delta m_{\text{sol}}^2} + \sqrt{\Delta m_{\text{atm}}^2}$  and

$$\left(m_{\nu_e}^{\text{eff}}\right)^2 = s_{12}^2 c_{13}^2 \Delta m_{\text{sol}}^2 + s_{13}^2 \Delta m_{\text{atm}}^2. \quad (4.2)$$

Moreover, due to our parametrization of the  $M_{\text{light}}$ , we get  $m_{ee} = \kappa$ . The ranges of these masses consistent with neutrino oscillation data, are shown in Tab. 3. The values of these effective masses are well below their corresponding experimental bounds.

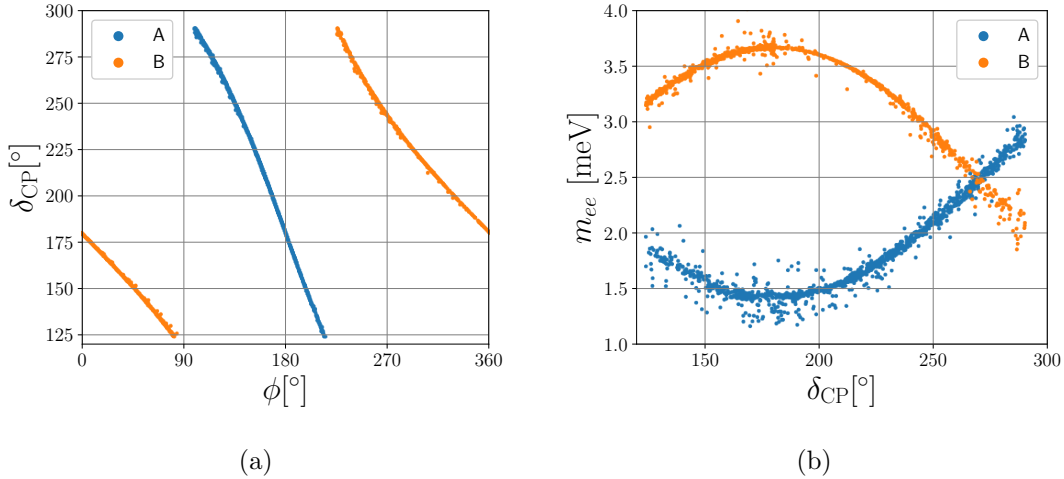


**Figure 3:** The relations between the free parameter  $\phi$  and  $\delta$  (a), and  $\delta$  and  $m_{ee}$  (b) in scenarios A and B.

In our framework, the parameter  $\phi$  is responsible for  $CP$  violation. We find a strong correlation between  $\phi$  and the Dirac phase  $\delta$  in both scenarios A and B, see Fig. 3 (a). We also observe an upper bound  $\delta \lesssim 290^\circ$  in both scenarios. More interestingly, we have identified a strong correlation between  $m_{ee}$  and  $\delta$ , see Fig. 3 (b). Their relationship can be well approximated by an empirical formula

$$m_{ee}^{(A)} = s_{12}^2 c_{13}^2 \sqrt{\Delta m_{\text{sol}}^2} + s_{13}^2 \sqrt{\Delta m_{\text{atm}}^2} \cos(\delta_{CP}), \quad (4.3)$$

$$m_{ee}^{(B)} = s_{12}^2 c_{13}^2 \sqrt{\Delta m_{\text{sol}}^2} + s_{13}^2 \sqrt{\Delta m_{\text{atm}}^2} \cos(\delta_{CP} + \pi). \quad (4.4)$$

For the DM and muon  $g - 2$  sector, we consider five free parameters: the DM mass ( $m_\chi$ ), the axion mass ( $m_a$ ), the axion decay constant ( $f_a$ ), the scalar mixing parameter ( $X_\Phi$ ), and the axion-fermion coupling coefficient ( $C_{ff}$ ). We aim to identify the parameter space consistent with three key observations: 1) the observed DM relic abundance, 2) the measured muon magnetic moment, and 3) the axion-top coupling search conducted by ATLAS.

Fig. 4 illustrates the allowed and excluded regions across various current constraints. The green region is excluded by recent muon  $g - 2$  measurements. The sky blue region represents the parameter space consistent with the thermal relic density, assuming the freeze-out approximation. The pink region indicates the exclusion limit derived from the ATLAS measurement of  $t\bar{t}$  production, which is used to constrain axion-top coupling. This measurement, detailed in Ref. [83], considered the lepton+jets channel with high- $p_T$  top quarks and an integrated luminosity of  $\mathcal{L} = 139 \text{ fb}^{-1}$ . Regions colored white indicate under-abundant DM, while dotted gold signifies over-abundant regions.

At DM masses less than 1 GeV, DM can annihilate into six primary channels:  $e^+e^-$ ,  $u\bar{u}$ ,  $d\bar{d}$ ,  $s\bar{s}$ ,  $\mu^+\mu^-$ , and  $c\bar{c}$ . Around the tau lepton mass ( $m_\tau$ ), annihilation into  $\tau^+\tau^-$  also becomes kinematically allowed. Similarly, as the DM mass increases further and exceeds

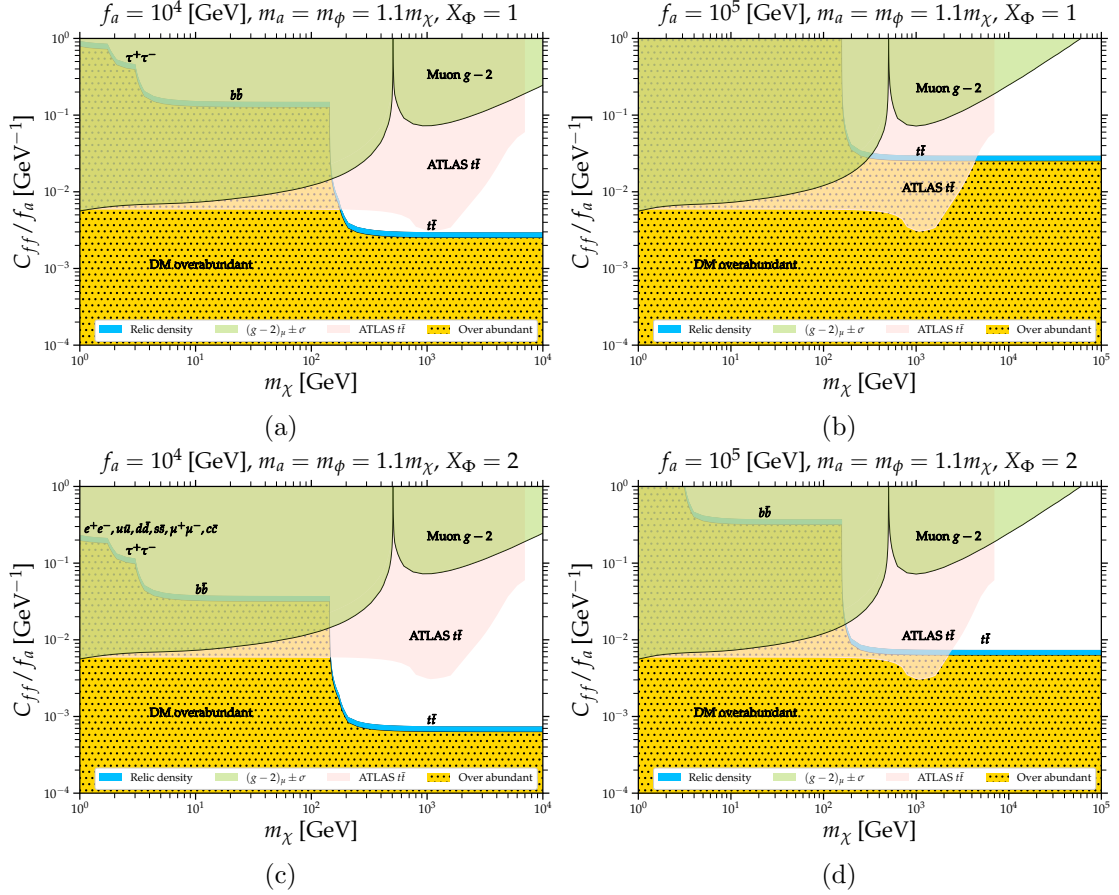


**Figure 4:** The plot of  $C_{ff}/f_a$  [GeV] $^{-1}$  and  $m_\chi$  [GeV] for  $m_a = m_\phi = 1.1m_\chi$ . The green colour labels the region excluded by latest  $g - 2$  within  $\pm\sigma$ . The pink colour represents the exclusion limit from the ATLAS measurement of  $t\bar{t}$  production. The sky blue region is allowed by thermal relic density. The white and dotted gold represent the under and over abundant regions, respectively. A pair of  $f\bar{f}$  label the dominant DM annihilation channel.

the bottom quark mass ( $m_b$ ) and top quark mass ( $m_t$ ), the  $b\bar{b}$  and  $t\bar{t}$  annihilation channels become kinematically accessible. According to the thermal DM annihilation cross-section, the ratio  $C_{ff}/f_a$  decreases as the DM mass increases. This trend is evident in Fig. 4; when these heavier quark channels open up, a smaller  $C_{ff}/f_a$  value is required to satisfy the relic density.

Figures 4(a) and (b) demonstrate that increasing  $f_a$  necessitates a corresponding increase in  $C_{ff}$ . This is because the ratio  $C_{ff}/f_a$  must remain constant for specific values of  $m_a$ ,  $m_\phi$ , and  $X_\Phi$  to maintain the relic density. In these plots, the most significant constraint comes from the ATLAS  $t\bar{t}$  search, which excludes DM masses below 180 GeV for  $f_a = 10^4$  GeV and below 4 TeV for  $f_a = 10^5$  GeV. When  $X_\Phi$  is doubled, as shown in Figures 4(c) and (d), the ratio  $C_{ff}/f_a$  must be suppressed by a factor of four, given that the annihilation cross-section scales as  $\langle\sigma v\rangle \propto (C_{ff}/f_a)^2 X_\Phi^4$ . However, this has only a mild effect on the allowed DM parameter space. After increasing  $X_\Phi$ , the allowed DM

mass range slightly expands to include masses up to 150 GeV for  $f_a = 10^4$  GeV and up to 2 TeV for  $f_a = 10^5$  GeV.

## 5 Conclusion and discussion

We presented a minimal extension of the SM that combines the inverse seesaw mechanism with an ALP portal DM. This model addresses both the origin of neutrino masses and the nature of DM while remaining consistent with current experimental constraints. Unlike traditional seesaw models that require high mass scales, the inverse seesaw mechanism allows for TeV-scale new physics, making it potentially accessible in future collider experiments. Additionally, the ALP serves as a mediator between the SM and DM sectors, providing a distinct phenomenology that includes a positive contribution to the muon anomalous magnetic moment ( $g - 2$ ) and compatibility with observed relic density.

From our analysis, we find two minimal scenarios for the inverse seesaw mechanism. They both lead to NO neutrinos with vanishing lightest neutrino mass. As a result, the total neutrino mass  $\sum_i m_i$  and the effective masses  $m_{\nu_e}^{eff}$  and  $m_{ee}$  are directly related to  $\Delta m_{sol}^2$  and  $\Delta m_{atm}^2$ . For the total neutrino mass, we find  $\sum_i m_i \simeq 58$  meV. This is an order of magnitude below the current Planck constraint. However, it can be probed by the Simon Observatory whose projected sensitivity is  $\sum_i m_i \leq 40$  meV at 95% CL [84]. Meanwhile, the effective mass  $m_{\nu_e}^{eff}$  in our scenarios are around 9 meV, which is an order of magnitude below the projection  $m_{\nu_e}^{eff} \leq 200$  meV at 90% CL of both the HOLMES and the KATRIN experiments [85, 86]. Moreover, we find the effective mass  $m_{ee}$  is of order a few meV. This is well below the projected sensitivity of  $m_{ee} \leq 13 - 29$  meV at 90% CL of the LEGEND experiment phase II [87]. Thus, the key signature for our neutrino sector is a signal in cosmological measurements ( $\sum_i m_i$ ) without corresponding signals in laboratory based measurements ( $m_{\nu_e}^{eff}$  and  $m_{ee}$ ).

In our scenario, the DM density is determined from the annihilation  $\chi\bar{\chi} \rightarrow f\bar{f}$  through a s-channel ALP exchange. For sufficiently large  $m_\chi$ , the  $t\bar{t}$  annihilation channel dominates over other di-fermion channels. In the benchmark scenario where  $m_a = m_\phi = 1.1m_\chi$ , we find that DM can be a thermal relic for  $m_a \gtrsim 150$  GeV, see Fig. 4. The ALP couplings that determine DM density also generate either a positive or a negative shift in the muon  $g - 2$ . We identify the region of parameter space in the  $m_a - C_{ff}/f_a$  plane which could explain the DM relic density, satisfy the muon  $g - 2$  and the ATLAS  $t\bar{t}$  constraints for  $f_a/[\text{GeV}] = 10^4, 10^5$  and  $X_\Phi = 1, 2$ , respectively. If neutrino and DM masses are generated through our scenario, the LHC Run 3 and/or HL-LHC data could probe the  $m_\chi \lesssim 2$  TeV regime for  $f_a = 10^4$  GeV scenario.

## Acknowledgement

This research has received funding support from the NSRF via the Program Management Unit for Human Resources & Institutional Development, Research and Innovation [grant number B13F670063]. CP is supported by Fundamental Fund 2567 of Khon Kaen University via the National Science Research and Innovation Fund (NSRF). The work of PU is

supported in part by the Mid-Career Research Grant from the National Research Council of Thailand under contract no. N42A650378. PU also thanks the High-Energy Physics Research Unit, Chulalongkorn University for hospitality while part of this work was being completed.

## References

- [1] SUPER-KAMIOKANDE collaboration, *Evidence for oscillation of atmospheric neutrinos*, *Phys. Rev. Lett.* **81** (1998) 1562 [[hep-ex/9807003](#)].
- [2] SNO collaboration, *Direct evidence for neutrino flavor transformation from neutral current interactions in the Sudbury Neutrino Observatory*, *Phys. Rev. Lett.* **89** (2002) 011301 [[nucl-ex/0204008](#)].
- [3] KAMLAND collaboration, *First results from KamLAND: Evidence for reactor anti-neutrino disappearance*, *Phys. Rev. Lett.* **90** (2003) 021802 [[hep-ex/0212021](#)].
- [4] DAYA BAY collaboration, *Measurement of Electron Antineutrino Oscillation Amplitude and Frequency via Neutron Capture on Hydrogen at Daya Bay*, *Phys. Rev. Lett.* **133** (2024) 151801 [[2406.01007](#)].
- [5] RENO collaboration, *Observation of Reactor Electron Antineutrino Disappearance in the RENO Experiment*, *Phys. Rev. Lett.* **108** (2012) 191802 [[1204.0626](#)].
- [6] CHOOZ collaboration, *Limits on neutrino oscillations from the CHOOZ experiment*, *Phys. Lett. B* **466** (1999) 415 [[hep-ex/9907037](#)].
- [7] K2K collaboration, *Indications of neutrino oscillation in a 250 km long baseline experiment*, *Phys. Rev. Lett.* **90** (2003) 041801 [[hep-ex/0212007](#)].
- [8] T2K collaboration, *Indication of Electron Neutrino Appearance from an Accelerator-produced Off-axis Muon Neutrino Beam*, *Phys. Rev. Lett.* **107** (2011) 041801 [[1106.2822](#)].
- [9] LSND collaboration, *Evidence for neutrino oscillations from the observation of  $\bar{\nu}_e$  appearance in a  $\bar{\nu}_\mu$  beam*, *Phys. Rev. D* **64** (2001) 112007 [[hep-ex/0104049](#)].
- [10] S. Weinberg, *Baryon and Lepton Nonconserving Processes*, *Phys. Rev. Lett.* **43** (1979) 1566.
- [11] R.N. Mohapatra and G. Senjanovic, *Neutrino Mass and Spontaneous Parity Nonconservation*, *Phys. Rev. Lett.* **44** (1980) 912.
- [12] J. Schechter and J.W.F. Valle, *Neutrino Masses in  $SU(2) \times U(1)$  Theories*, *Phys. Rev. D* **22** (1980) 2227.
- [13] S.F. King, *Neutrino mass models*, *Rept. Prog. Phys.* **67** (2004) 107 [[hep-ph/0310204](#)].
- [14] R.N. Mohapatra and J.W.F. Valle, *Neutrino Mass and Baryon Number Nonconservation in Superstring Models*, *Phys. Rev. D* **34** (1986) 1642.
- [15] P.S.B. Dev and A. Pilaftsis, *Minimal Radiative Neutrino Mass Mechanism for Inverse Seesaw Models*, *Phys. Rev. D* **86** (2012) 113001 [[1209.4051](#)].
- [16] S.F. King and C. Luhn, *Neutrino Mass and Mixing with Discrete Symmetry*, *Rept. Prog. Phys.* **76** (2013) 056201 [[1301.1340](#)].
- [17] F.F. Deppisch, P.S. Bhupal Dev and A. Pilaftsis, *Neutrinos and Collider Physics*, *New J. Phys.* **17** (2015) 075019 [[1502.06541](#)].

- [18] M.B. Gavela, T. Hambye, D. Hernandez and P. Hernandez, *Minimal Flavour Seesaw Models*, *JHEP* **09** (2009) 038 [[0906.1461](#)].
- [19] A. Ibarra, E. Molinaro and S.T. Petcov, *TeV Scale See-Saw Mechanisms of Neutrino Mass Generation, the Majorana Nature of the Heavy Singlet Neutrinos and  $(\beta\beta)_{0\nu}$ -Decay*, *JHEP* **09** (2010) 108 [[1007.2378](#)].
- [20] F. Deppisch and J.W.F. Valle, *Enhanced lepton flavor violation in the supersymmetric inverse seesaw model*, *Phys. Rev. D* **72** (2005) 036001 [[hep-ph/0406040](#)].
- [21] P.S.B. Dev and R.N. Mohapatra, *TeV Scale Inverse Seesaw in  $SO(10)$  and Leptonic Non-Unitarity Effects*, *Phys. Rev. D* **81** (2010) 013001 [[0910.3924](#)].
- [22] A. Das and N. Okada, *Inverse seesaw neutrino signatures at the LHC and ILC*, *Phys. Rev. D* **88** (2013) 113001 [[1207.3734](#)].
- [23] C. Bonilla, A.E. Carcamo Hernandez, B. Saez Diaz, S. Kovalenko and J. Marchant Gonzalez, *Dark matter from a radiative inverse seesaw majoron model*, *Phys. Lett. B* **847** (2023) 138282 [[2306.08453](#)].
- [24] P. Bharadwaj, R. Kumar, H.K. Prajapati, R. Srivastava and S. Yadav, *Dark Matter Escaping Direct Detection Runs into Higgs Mass Hierarchy Problem*, [2412.13301](#).
- [25] P. Langacker, *Grand Unified Theories and Proton Decay*, *Phys. Rept.* **72** (1981) 185.
- [26] S. Davidson, E. Nardi and Y. Nir, *Leptogenesis*, *Phys. Rept.* **466** (2008) 105 [[0802.2962](#)].
- [27] G. Altarelli and F. Feruglio, *Discrete Flavor Symmetries and Models of Neutrino Mixing*, *Rev. Mod. Phys.* **82** (2010) 2701 [[1002.0211](#)].
- [28] A. Abada and M. Lucente, *Looking for the minimal inverse seesaw realisation*, *Nucl. Phys. B* **885** (2014) 651 [[1401.1507](#)].
- [29] S. Alekhin et al., *A facility to Search for Hidden Particles at the CERN SPS: the SHiP physics case*, *Rept. Prog. Phys.* **79** (2016) 124201 [[1504.04855](#)].
- [30] J. Hisano, T. Moroi, K. Tobe and M. Yamaguchi, *Lepton flavor violation via right-handed neutrino Yukawa couplings in supersymmetric standard model*, *Phys. Rev. D* **53** (1996) 2442 [[hep-ph/9510309](#)].
- [31] Y. Kuno and Y. Okada, *Muon decay and physics beyond the standard model*, *Rev. Mod. Phys.* **73** (2001) 151 [[hep-ph/9909265](#)].
- [32] J. Beacham et al., *Physics Beyond Colliders at CERN: Beyond the Standard Model Working Group Report*, *J. Phys. G* **47** (2020) 010501 [[1901.09966](#)].
- [33] PARTICLE DATA GROUP collaboration, *Review of particle physics*, *Phys. Rev. D* **110** (2024) 030001.
- [34] G. Bertone, D. Hooper and J. Silk, *Particle dark matter: Evidence, candidates and constraints*, *Phys. Rept.* **405** (2005) 279 [[hep-ph/0404175](#)].
- [35] PLANCK collaboration, *Planck 2018 results. VI. Cosmological parameters*, *Astron. Astrophys.* **641** (2020) A6 [[1807.06209](#)].
- [36] WMAP collaboration, *First year Wilkinson Microwave Anisotropy Probe (WMAP) observations: Determination of cosmological parameters*, *Astrophys. J. Suppl.* **148** (2003) 175 [[astro-ph/0302209](#)].

- [37] COBE collaboration, *Structure in the COBE differential microwave radiometer first year maps*, *Astrophys. J. Lett.* **396** (1992) L1.
- [38] J.L. Feng, *Dark Matter Candidates from Particle Physics and Methods of Detection*, *Ann. Rev. Astron. Astrophys.* **48** (2010) 495 [[1003.0904](#)].
- [39] G. Arcadi, M. Dutra, P. Ghosh, M. Lindner, Y. Mambrini, M. Pierre et al., *The waning of the WIMP? A review of models, searches, and constraints*, *Eur. Phys. J. C* **78** (2018) 203 [[1703.07364](#)].
- [40] G. Bertone and T. Tait, M. P., *A new era in the search for dark matter*, *Nature* **562** (2018) 51 [[1810.01668](#)].
- [41] M. Cirelli, A. Strumia and J. Zupan, *Dark Matter*, [2406.01705](#).
- [42] N. Bozorgnia, J. Bramante, J.M. Cline, D. Curtin, D. McKeen, D.E. Morrissey et al., *Dark Matter Candidates and Searches*, [2410.23454](#).
- [43] C. Balazs, T. Bringmann, F. Kahlhoefer and M. White, *A Primer on Dark Matter*, [2411.05062](#).
- [44] B. Patt and F. Wilczek, *Higgs-field portal into hidden sectors*, [hep-ph/0605188](#).
- [45] A. Djouadi, O. Lebedev, Y. Mambrini and J. Quevillon, *Implications of LHC searches for Higgs-portal dark matter*, *Phys. Lett. B* **709** (2012) 65 [[1112.3299](#)].
- [46] F. Bishara, J. Brod, P. Uttayarat and J. Zupan, *Nonstandard Yukawa Couplings and Higgs Portal Dark Matter*, *JHEP* **01** (2016) 010 [[1504.04022](#)].
- [47] G. Arcadi, A. Djouadi and M. Raidal, *Dark Matter through the Higgs portal*, *Phys. Rept.* **842** (2020) 1 [[1903.03616](#)].
- [48] M. Dine, W. Fischler and M. Srednicki, *A Simple Solution to the Strong CP Problem with a Harmless Axion*, *Phys. Lett. B* **104** (1981) 199.
- [49] R.D. Peccei and H.R. Quinn, *CP Conservation in the Presence of Instantons*, *Phys. Rev. Lett.* **38** (1977) 1440.
- [50] S. Weinberg, *A New Light Boson?*, *Phys. Rev. Lett.* **40** (1978) 223.
- [51] Y. Nomura and J. Thaler, *Dark Matter through the Axion Portal*, *Phys. Rev. D* **79** (2009) 075008 [[0810.5397](#)].
- [52] M. Freytsis, Z. Ligeti and J. Thaler, *Constraining the Axion Portal with  $B \rightarrow Kl^+l^-$* , *Phys. Rev. D* **81** (2010) 034001 [[0911.5355](#)].
- [53] M. Bauer, G. Rostagni and J. Spinner, *Axion-Higgs portal*, *Phys. Rev. D* **107** (2023) 015007 [[2207.05762](#)].
- [54] A.S. Zhevlakov, D.V. Kirpichnikov and V.E. Lyubovitskij, *Implication of the dark axion portal for the EDM of fermions and dark matter probing with NA64e, NA64 $\mu$ , LDMX, M3, and BaBar*, *Phys. Rev. D* **106** (2022) 035018 [[2204.09978](#)].
- [55] C.D.R. Carvalho, A.G. Dias, C.C. Nishi and B.L. Sánchez-Vega, *Axion Like Particles and the Inverse Seesaw Mechanism*, *JHEP* **05** (2015) 069 [[1503.03502](#)].
- [56] MUON G-2 collaboration, *Measurement of the Positive Muon Anomalous Magnetic Moment to 0.46 ppm*, *Phys. Rev. Lett.* **126** (2021) 141801 [[2104.03281](#)].
- [57] MUON G-2 collaboration, *Measurement of the Positive Muon Anomalous Magnetic Moment to 0.20 ppm*, *Phys. Rev. Lett.* **131** (2023) 161802 [[2308.06230](#)].

- [58] MUON G-2 collaboration, *Final Report of the Muon E821 Anomalous Magnetic Moment Measurement at BNL*, *Phys. Rev. D* **73** (2006) 072003 [[hep-ex/0602035](#)].
- [59] T. Aoyama et al., *The anomalous magnetic moment of the muon in the Standard Model*, *Phys. Rept.* **887** (2020) 1 [[2006.04822](#)].
- [60] R. Aliberti et al., *The anomalous magnetic moment of the muon in the Standard Model: an update*, [2505.21476](#).
- [61] MUON G-2 collaboration, *Measurement of the Positive Muon Anomalous Magnetic Moment to 127 ppb*, [2506.03069](#).
- [62] C. Pongkitivanichkul, N. Thongyoi and P. Uttayarat, *Inverse seesaw mechanism and portal dark matter*, *Phys. Rev. D* **100** (2019) 035034 [[1905.13224](#)].
- [63] P.J. Fitzpatrick, Y. Hochberg, E. Kuflik, R. Ovadia and Y. Soreq, *Dark matter through the axion-gluon portal*, *Phys. Rev. D* **108** (2023) 075003 [[2306.03128](#)].
- [64] G. Armando, P. Panci, J. Weiss and R. Ziegler, *Leptonic ALP portal to the dark sector*, *Phys. Rev. D* **109** (2024) 055029 [[2310.05827](#)].
- [65] D.K. Ghosh, A. Ghoshal and S. Jeusun, *Axion-like particle (ALP) portal freeze-in dark matter confronting ALP search experiments*, *JHEP* **01** (2024) 026 [[2305.09188](#)].
- [66] J.C. Gutiérrez, B.J. Kavanagh, N. Castelló-Mor, F.J. Casas, J.M. Diego, E. Martínez-González et al., *Cosmology and direct detection of the Dark Axion Portal*, [2112.11387](#).
- [67] F.P. Di Meglio, *Visible QCD Axion Portal to a Dark Sector*, Master's thesis, Pisa U., 2021.
- [68] S. Gola, S. Mandal and N. Sinha, *ALP-portal majorana dark matter*, *Int. J. Mod. Phys. A* **37** (2022) 2250131 [[2106.00547](#)].
- [69] P. Deniverville, H.-S. Lee and Y.-M. Lee, *New searches at reactor experiments based on the dark axion portal*, *Phys. Rev. D* **103** (2021) 075006 [[2011.03276](#)].
- [70] D.V. Kirpichnikov, V.E. Lyubovitskij and A.S. Zhevlakov, *Implication of hidden sub-GeV bosons for the  $(g-2)_\mu$ ,  $^8\text{Be-}^4\text{He}$  anomaly, proton charge radius, EDM of fermions, and dark axion portal*, *Phys. Rev. D* **102** (2020) 095024 [[2002.07496](#)].
- [71] P. deNiverville and H.-S. Lee, *Implications of the dark axion portal for SHiP and FASER and the advantages of monophoton signals*, *Phys. Rev. D* **100** (2019) 055017 [[1904.13061](#)].
- [72] P. deNiverville, H.-S. Lee and M.-S. Seo, *Implications of the dark axion portal for the muon  $g-2$ , B factories, fixed target neutrino experiments, and beam dumps*, *Phys. Rev. D* **98** (2018) 115011 [[1806.00757](#)].
- [73] K. Kaneta, H.-S. Lee and S. Yun, *Dark photon relic dark matter production through the dark axion portal*, *Phys. Rev. D* **95** (2017) 115032 [[1704.07542](#)].
- [74] CMS collaboration, *A portrait of the Higgs boson by the CMS experiment ten years after the discovery*, *Nature* **607** (2022) 60 [[2207.00043](#)].
- [75] ATLAS collaboration, *A detailed map of Higgs boson interactions by the ATLAS experiment ten years after the discovery*, *Nature* **607** (2022) 52 [[2207.00092](#)].
- [76] C.B. Adams et al., *Axion Dark Matter*, in *Snowmass 2021*, 3, 2022 [[2203.14923](#)].
- [77] I. Esteban, M.C. Gonzalez-Garcia, M. Maltoni, I. Martinez-Soler, J.a.P. Pinheiro and

- T. Schwetz, *NuFit-6.0: Updated global analysis of three-flavor neutrino oscillations*, [2410.05380](#).
- [78] E.E. Jenkins and A.V. Manohar, *Rephasing Invariants of Quark and Lepton Mixing Matrices*, *Nucl. Phys. B* **792** (2008) 187 [[0706.4313](#)].
- [79] KATRIN collaboration, *Direct neutrino-mass measurement based on 259 days of KATRIN data*, [2406.13516](#).
- [80] KAMLAND-ZEN collaboration, *Search for the Majorana Nature of Neutrinos in the Inverted Mass Ordering Region with KamLAND-Zen*, *Phys. Rev. Lett.* **130** (2023) 051801 [[2203.02139](#)].
- [81] M.A. Buen-Abad, J. Fan, M. Reece and C. Sun, *Challenges for an axion explanation of the muon  $g - 2$  measurement*, *JHEP* **09** (2021) 101 [[2104.03267](#)].
- [82] S. Ganguly, B. Mukhopadhyaya and S. Roy, *Can leptophilic-ALP be a solution to the muon  $(g - 2)$  anomaly?*, [2204.07920](#).
- [83] F. Esser, M. Madigan, V. Sanz and M. Ubiali, *On the coupling of axion-like particles to the top quark*, *JHEP* **09** (2023) 063 [[2303.17634](#)].
- [84] SIMONS OBSERVATORY collaboration, *The Simons Observatory: Astro2020 Decadal Project Whitepaper*, *Bull. Am. Astron. Soc.* **51** (2019) 147 [[1907.08284](#)].
- [85] B. Alpert et al., *HOLMES - The Electron Capture Decay of  $^{163}\text{Ho}$  to Measure the Electron Neutrino Mass with sub-eV sensitivity*, *Eur. Phys. J. C* **75** (2015) 112 [[1412.5060](#)].
- [86] KATRIN collaboration, *Improved Upper Limit on the Neutrino Mass from a Direct Kinematic Method by KATRIN*, *Phys. Rev. Lett.* **123** (2019) 221802 [[1909.06048](#)].
- [87] LEGEND collaboration, *The Large Enriched Germanium Experiment for Neutrinoless Double Beta Decay (LEGEND)*, *AIP Conf. Proc.* **1894** (2017) 020027 [[1709.01980](#)].